Geologie en Mijnbouw **71**: 23–32, 1992.

Quantification of pore geometry in carbonates using image analysis; Upper Permian (Zechstein) of Denmark

Peter Frykman
Geological Survey of Denmark, Thoravej 8, DK-2400 Copenhagen NV, Denmark

Received 5 September 1991; accepted in revised form 7 March 1992

Key words: hydrocarbon reservoirs, Løgumkloster-1

Abstract

Image analysis of Permian Zechstein carbonate samples has aided quantification of pore geometry parameters. Total porosity has been measured, using image analysis, from randomly selected thin sections. These porosity measurements have then been compared to core analysis measurements of the same samples.

Pore surface parameters derived from the image analysis can be used to characterize mouldic porosity, and to estimate permeability. Cumulative porosity curves related to pore section size are used to group the samples in classes with different pore geometry.

Introduction

Reservoir properties of rocks are largely determined by pore geometries. Qualitative description of pore geometry and measurements of connectivity have so far been used to characterize the porous networks. Recent advances in computerized image analysis have provided a way to quantify pore geometries, and to enable a more detailed characterization of the network properties. Image analysis is used to characterize pore geometry from random thin sections. Several different strategies have been used to obtain parameters for the two-dimensional textural character of the pore space (e.g., Bisdom *et al.*1983, Dilks and Graham 1985, Ehrlich *et al.* 1984, 1991, Ruzyla 1986, Yuan 1990, Habesch 1990).

From thin sections, only two-dimensional descriptions can be given of the pore geometry parameters, whereas some bulk material properties can be quantified directly.

Bulk material properties like porosity percentage and total pore surface area are easily derived from image analysis. Quantification of parameters for the three-dimensional porous network from thin sections is difficult to obtain by the procedure described here, although methods have been suggested by Dullien and Dhawan (1973, 1974).

The most important types of porosity in the Zechstein carbonates studied are microporosity and oomouldic porosity. These porosity types have an impact on log-interpretation. The isolated, spherical, poorly connected nature of oomouldic porosity affects the response of the sonic log, causing it to read a lower porosity than measured by the neutron log. An aim of this study was to quantify the amount of oomouldic porosity by using image analysis.

Along with pore geometry, compositional data have also been obtained. Using backscattered electron (BSE) detection on a scanning electron microscope (SEM), several components can be distinguished by their different reflection coefficients. Dolomite and anhydrite are the main mineral components in the thin sections studied. Accessory minerals like pyrite and celestite are also observed.

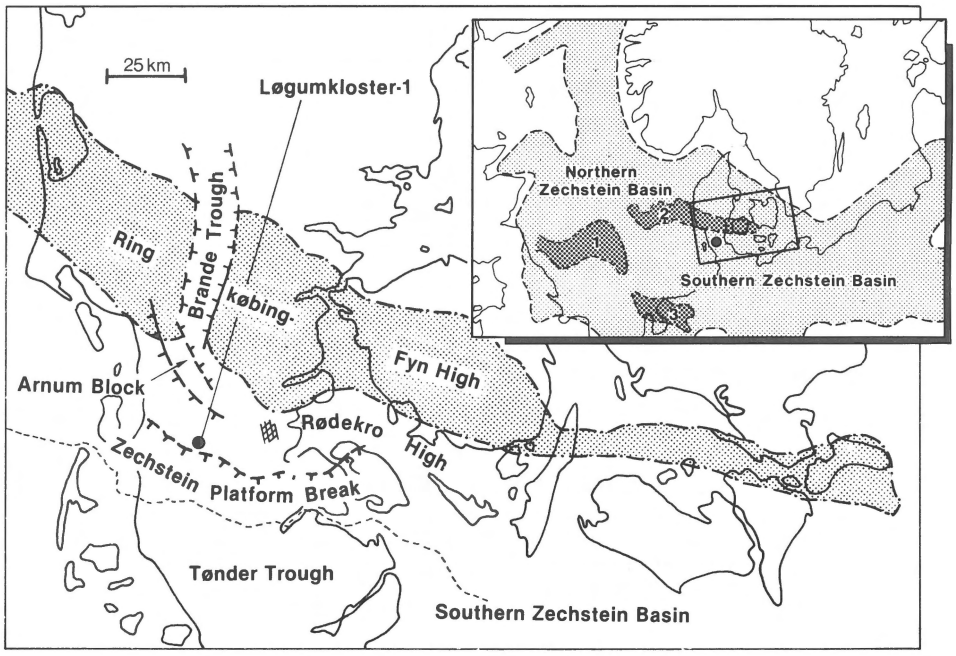

Fig. 1. Map showing the main structural elements in southern Denmark. The Zechstein platform was formed along the southern flank of the Ringkøbing-Fyn High. Material has been investigated from Ca-2 platform margin carbonates in the Løgumkloster-1 well.

The anhydrite content observed in thin section is quantified by image analysis.

Material

The material studied is taken from the Zechstein Ca-2 carbonate unit (Upper Permian) in the Løgumkloster-1 well in southern Denmark (Fig. 1). The Ca-2 unit is a dolomitized sequence including facies types from oolite shoals, lagoonal environments and intertidal marginal marine environments (Fig. 2). These facies reflect deposition on a carbonate platform where the oolite shoals were positioned at the seaward margin of the shallow water platform (Frykman et al. 1989, Stemmerik and Frykman 1989).

Diagenetic porosity evolution

The complex diagenesis of the Ca-2 carbonates is outlined in detail by Stentoft and Nygaard (1986) and Stentoft (1990), and is only briefly outlined here.

The original carbonate sediment was composed of a mixture of aragonite and Mg-calcite. An early fresh-water leaching phase created most of the secondary mouldic porosity in the carbonates.

A later, second dissolution phase affected the dolomite cement, creating intracrystalline porosity, and enlarged the existing secondary porosity. This late dissolution phase is thought to be related to the influx of CO_2 derived from maturation of organic matter. A minor phase of late dolomite cementation occurred. The most important late-diagenetic step is the precipitation of anhydrite cement from brines derived from the surrounding sulphate deposits. The anhydrite both replaced and cemented the carbonates, and forms the overriding factor that determines the amount of porosity in the carbonate unit. Oil entered the pore system at a late stage in the diagenetic evolution and was therefore highly depending on the pore geometry and degree of anhydritization.

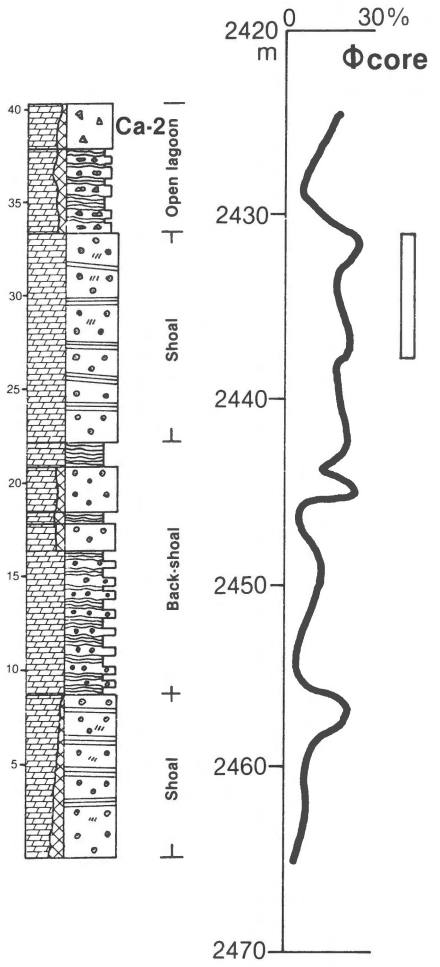

Fig. 2. Sedimentological log of the core material in the Ca-2 carbonate interval (2424–2465 m.b.KB.) from the Løgumkloster-1 well with the interpreted sedimentary environments. The measured core-porosity is shown as curve; the bar indicates a hydrocarbon-productive interval (from Stemmerik and Frykman 1989).

Porosity types

Two main types of porosity found in the investigated Zechstein core material are primary intergranular porosity and secondary mouldic porosity.

Primary intergranular porosity is the space between grains not occupied by finegrained matrix. A high energy level produces a well sorted sediment with little finegrained matrix. This porosity is characteristic of oolite shoals (Figs 3, 4) and in facies where a muddy matrix is absent.

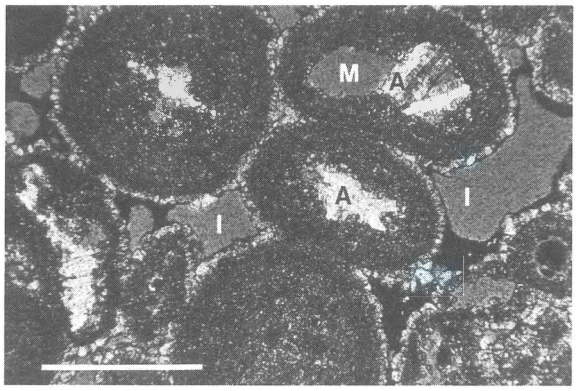

Fig. 3. Microphotograph showing remnant primary intergranular porosity (I) and mouldic porosity formed within the ooids (M), partly occluded by anhydrite (A). Sample from 2439.40 m.b.KB. Scale bar 0.5 mm.

Secondary mouldic porosity is formed by the selective dissolution of certain grain components in the rocks, e.g., ooids, oncoids or skeletal material (Figs 3–5). Components made of unstable mineralogies like aragonite and high-magnesium calcite

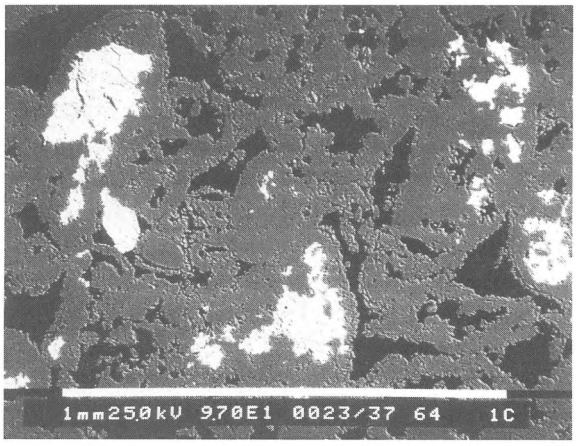

Fig. 4. Scanning microscope photograph obtained with backscattered electron detection (BSE). The white phase is anhydrite, grey is dolomite, black is porosity. The large pores are mainly intergranular. Some mouldic porosity inside the ooids is filled with diagenetic anhydrite. Sample 1C, 2424.00 m.b.KB. White scale bar is 1 mm.

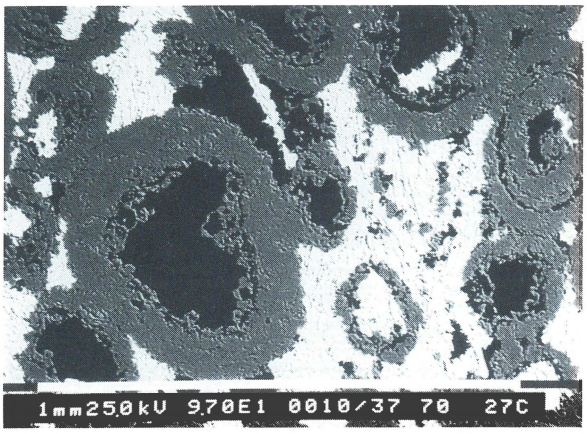

Fig. 5. BSE-picture showing large oomouldic pores. As in Fig. 4 the light material is anhydrite, grey is dolomite and dark is epoxy-filled pore-space. The anhydrite has mainly filled the intergranular pore-space. Sample 27, 2437.00 m.b.KB. White scale bar 1 mm.

are especially susceptible to dissolution. But, also relatively stable components made of calcite can be dissolved. Even individual generations of cement may be dissolved. This porosity is poorly connected and therefore contributes little to permeability.

Image analysis methodology

Vertical plugs ca. 25 mm (1″) in diameter have been drilled from the core, rinsed for hydrocarbons and salt, and dried. The plugs were impregnated with epoxy resin and then thin-sections were produced. The thin sections were taken vertically, polished and then carbon-coated for the use in SEM. The epoxy impregnation procedure was critical, to ensure that even the smallest pore space was filled. Pressure impregnation was therefore used to ensure good penetration. The small pores were difficult to impregnate and some relief is present on the polished sections. Fortunately, the BSE detection is not very sensitive to these disturbances, and the pore outlines are relatively clear (Figs 4, 5).

The SEM used is a Philips SEM 515 equipped with two BSE scintillation detectors. The largest field-of-view of the images with uniform illumination is approximately 750 × 750 microns at a magnification of ca. 100 ×. To obtain images of the micropores the magnification is raised to 800 x. The SEM electron beam was set at largest spot size, being 0,5 micron. Acceleration voltage is 25 KV.

Photographs were taken at slow-scan mode. Paperprints in standard size 9 × 13 cm were then used for input for the image analyser. In each sample at least 20 non-overlapping micro-photographs were taken, distributed over a total area of the slide covering c. 16 × 21 mm on the sample surface. With 10–20 fields measured, the analysed total area comprises 4–9 mm^2.

The image analyser equipment at the Geological Survey of Denmark is a Kontron IBAS I + II. A videocamera is fitted on a macrostand where the photographs are placed. The photograph is digitized into an image with a spatial resolution of 512 × 512 and an 8-bit grey level resolution (256 grey values).

The image analyser system works with user-defined program strings composed of functions selected from a library. Some of the functions are interactive during the actual analysis. The IBAS system uses a vector-processor for the calculation and measuring procedures, which gives a fast performance of the data collection.

Image analysis procedures

A main part of the image analysis procedure is to enhance the image and discriminate between the phases that are to be measured on the BSE-picture (Figs 4, 5). Initially the image is modified to obtain better contrast. Normalization of the original grey-tone-range of the image (Fig. 6A) is performed by a tone-expansion to the full grey-level range of 256 grey levels (Fig. 6B). Additionally a delineation function is performed to give better definition of contacts between different phases. Finally, a medium filter is applied removing noise seen as pore-areas less than 3 × 3 pixels. From this optimized image, the different components are discriminated by selecting the grey-level ranges representing the different phases. This discrimination can be controlled interactively for each image, and is facilitated by the grey-level histogram where the phases are represented as peaks and ranges (Fig. 6B).

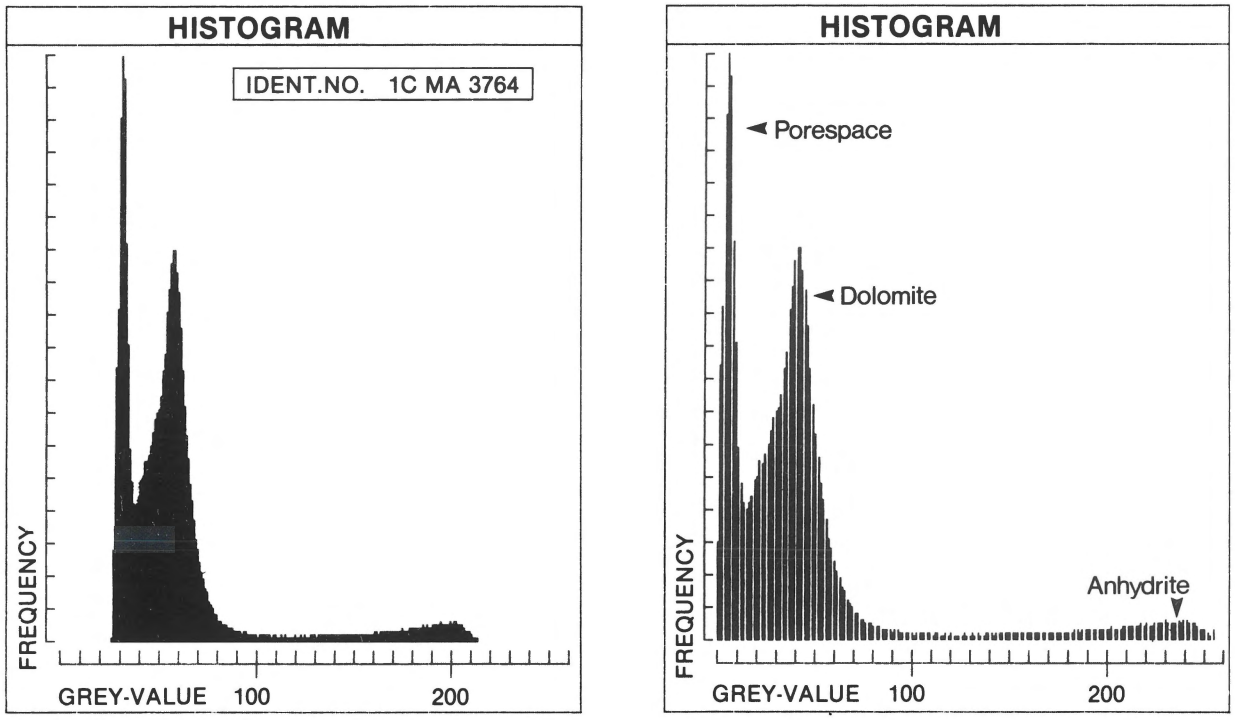

Fig. 6. A): Histogram of grey-level distribution in a frame-grabbed image of a BSE-picture. The full scale of 0–255 grey tones is not used by the image. B): Histogram of grey-level distribution in the image enhanced by NORMGREY function. The original content is expanded isotropically to exploit the full scale of grey tones. The peaks for the main components are indicated.

The grey-level histogram illustrates the difficulties arising from microporous areas in the sample. Microporosity is registered as a grey-level range between that for macropores and carbonate (Fig. 6B). This is due to blurring of the micropore boundaries with the carbonate phase. The anhydrite shows a well separated peak at the light end of the grey-scale (Fig. 6B). The macroporosity is defined with interactive control into a binary image of the macropores and the following parameters are measured in the selected field of view:

Reference area – area of field of view measured.
Field perimeter – total perimeter of the pore-section boundaries in the field of view.
Field area – area of total porespace in the field of view.
Area % – the percentage of porespace in the field of view.

The surface-related parameters Surface Density and Specific Surface are calculated from perimeter data. The area % derived from image analysis is directly comparable to volume % porosity. The anhydrite volume is also measured using this procedure.

The porosity measured from image analysis of 2D sections is readily derived from the area measurements by the relationship:

$$\varnothing = \mathrm{Vol}_{\mathrm{pore}}/\mathrm{Vol}_{\mathrm{total}} = \mathrm{Area}_{\mathrm{pore}}/\mathrm{Area}_{\mathrm{total}} \qquad (1)$$

This quantifies the principle given by Delesse (1847) and further expressed by Rink and Schopper (1978). The relation assumes that the spatial pore distribution is statistically homogeneous and isotropic.

The measurement of parameters specific for the individual pore sections requires an identification of the separate pore sections. The identification is also necessary in order to deal with pore sections extending outside the sample field, and to ensure

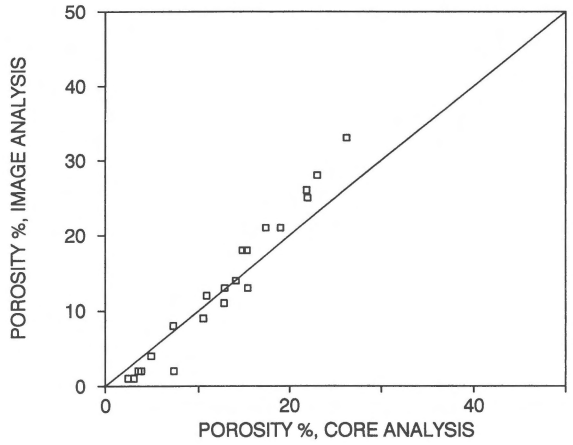

Fig. 7. Crossplot of porosity values determined by core-analysis (Helium-porosimetry) and image analysis. A good correlation is present, except for the high porosity values where isolated porosity seemingly is not fully detected by the He-porosimetry.

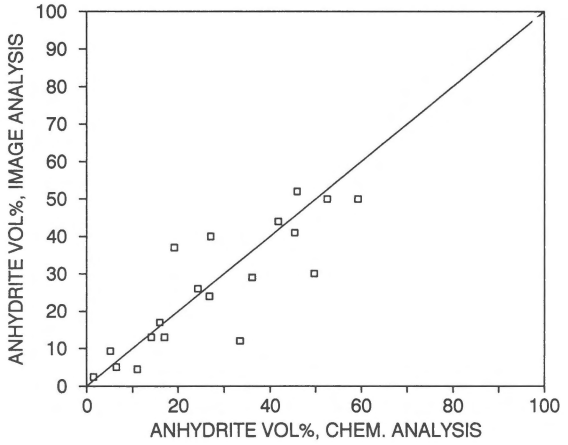

Fig. 8. Crossplot of anhydrite content as measured by standard chemical analysis and by image analysis.

statistic representation of the pore section data. The sample field is smaller than the total field of view and is limited by a measuring frame. Pore sections touching any of two connected sides of the measuring frame are eliminated by the identification process, whereas pore sections touching the two opposite sides of the frame are identified with their full extension also if they are reaching outside the measuring frame. The use of such discrimination tools has been discussed by Gundersen (1986).

The following parameters are measured for the individual pore sections:

Area – proportional to number of pixels.
Perimeter.
Minimum diameter – minimum value of feret diameters (calipers) measured in 32 projections.

Sources of error:

The accuracy of the measurements depends on several factors:
BSE detection volume (spot diameter 0.5 × 1 micron depth).
Boundary wedging effects.
Film/print quality.
Video-framegrabbing resolution.
Image modifications and enhancement.
Discrimination of analyzed phase.
Measuring precision of equipment.

The BSE detection volume is only critical for imaging the microporosity, where pores less than 10 micron diameter are studied at a magnification of 800 ×.

Image modifications with the image analysis program are important, especially for the shape-dependent measurements like perimeter. Application of smoothing functions is critical to such parameters. The commonly used procedure of erosion/dilation has not been applied during this work. This is because emphasis has been placed on obtaining pore surface related parameters like Surface Density and Specific Surface.

The discrimination procedure of the pore fraction is performed interactively for all samples in each sample series. The grey-level histogram (Fig. 6B) helps in this procedure but cannot, with the present material, be the basis for an automatic discrimination function. The accuracy of the equipment is found to be ± 1% when analyzing the same field 20 times.

The accuracy of measuring porosity % depends on the discrimination procedure, but is judged to be in the order of ± 2% (absolute%). When turning to the object-related measurements, the dis-

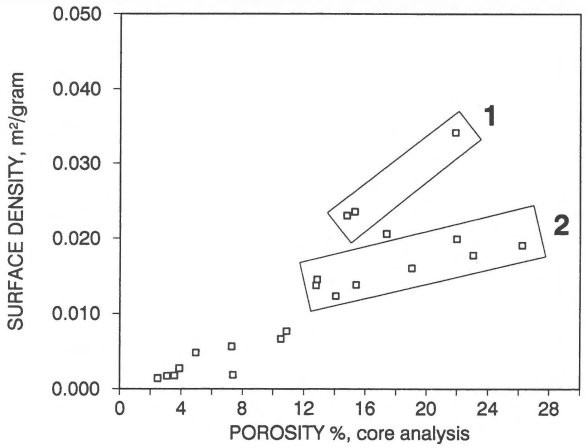

Fig. 9. Surface Density (pore surface related to sample weight) plotted with porosity %. Cluster 1 = many small pores and no mouldic porosity. Cluster 2 = oomouldic porosity/large intergranular porosity.

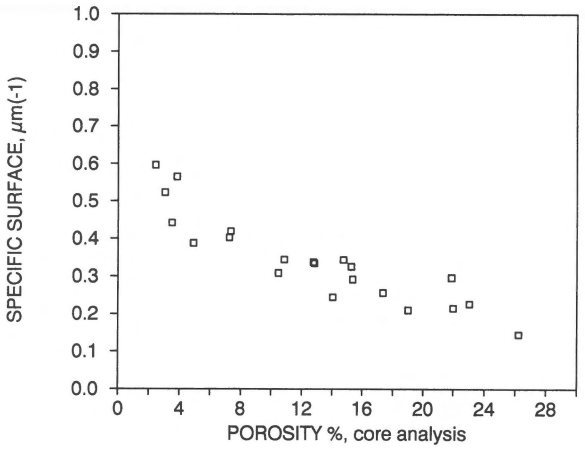

Fig. 10. Specific Surface (pore surface related to pore volume) plotted with porosity. A clear negative correlation is seen.

crimination procedure will have some influence on the size/shape parameters. However, the relative comparison of data within the material suite is still considered to be relevant.

With the present material, the limits of low magnification on the SEM have introduced an underrepresentation of the largest pores (>200 micron in diameter), because they often extend outside the field of view. Therefore their object-related parameters are not accurate. These large pores only occur in very few samples, but it illustrates the problem of measuring pore-sections where pore sizes are spread over several orders of magnitudes.

Results

Bulk measurements

The results from image analysis measurements of porosity % are compared with the porosity measured from the plugs by conventional core analysis. The comparison is shown on the crossplot in Fig. 7. Minor deviations are seen, mostly in the most porous samples where image analysis tends to give higher values. In the most porous samples, heterogeneity plays a major role. Also, isolated porosity has probably not been fully detected in the laboratory with the standard core-analysis, but it has been registered by image analysis. The wedging effect of the pore boundaries to the matrix and the BSE detection might be responsible for an underrepresentation at low porosities and an overestimation at high porosities.

The anhydrite content is also measured, and crossplotted with the chemical analyses on Fig. 8. Although some samples show deviation, a fair correlation is seen in most samples measured. The large deviations are likely to be the result of the

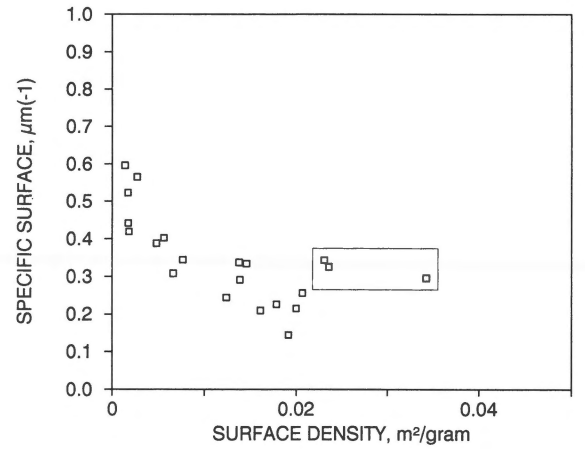

Fig. 11. Crossplot of Surface Density against Specific Surface. The sample suite lacking mouldic pores forms a separate cluster (box).

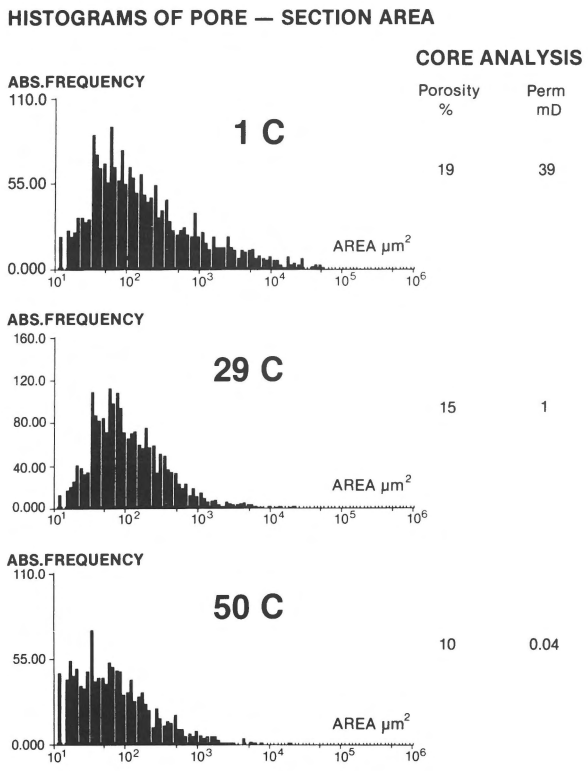

Fig. 12. Distribution histograms of the pore section areas measured on three samples, each including ca. 2000 individual pore sections. Porosity and permeability are listed for each sample.

heterogeneity of anhydrite distribution in the samples.

The calculated Surface Density (pore surface related to sample weight, Fig. 9), and Specific Surface (pore surface related to pore volume, Fig. 10), show variations that are related to total porosity and pore geometry. The crossplot of Surface Density and Specific Surface (Fig. 11) gives a general decline curve with a few samples of high Surface Density.

Pore section measurements

All measured parameters related to individual pore sections are expressed as distribution histograms (see examples on Fig. 12). Statistical analyses of the pore section area histograms give values for mean, standard deviation and skewness. The mean values

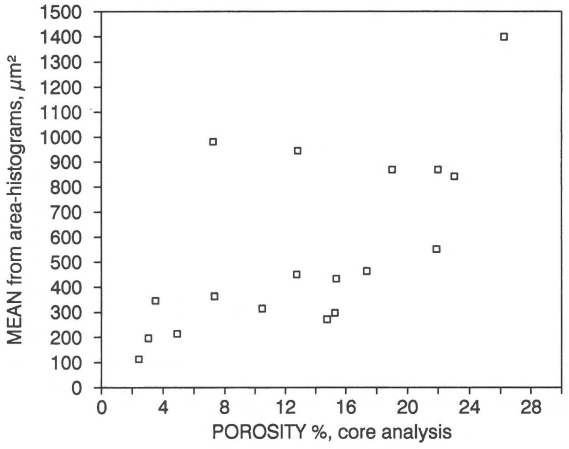

Fig. 13. Crossplot of area histogram means against core porosity showing a vague positive correlation.

have been related to total porosity (Fig. 13), which shows a slight positive correlation.

The pore area distributions can also be re-calculated as cumulative curves (Fig. 14). This procedure serves to accentuate the relative distribution of the pore area classes existing in the material.

Discussion

The plot of Surface Density (Fig. 9) shows two clusters in the high porosity range (>12%). Cluster 1 (Fig. 9) with relatively high Surface Density, includes samples that have many small and secondary pores and some needle-texture in the dolomite (samples 15, 18, 29). Cluster 2 includes samples having oomouldic or large intergranular pores. These have relatively non-folded surfaces and therefore contribute less to the surface density. On the plot of Specific Surface (Fig. 10) there is no obvious indication of two clusters in the material.

From the 21 samples investigated it has not been possible to detect any correlation of pore geometry with facies.

The expression of the pore section area distribution by the values for mean, standard deviation and skewness has not shown any recognizable systematic variations.

The cumulative pore area curves can be used to differentiate classes of pore geometries. For exam-

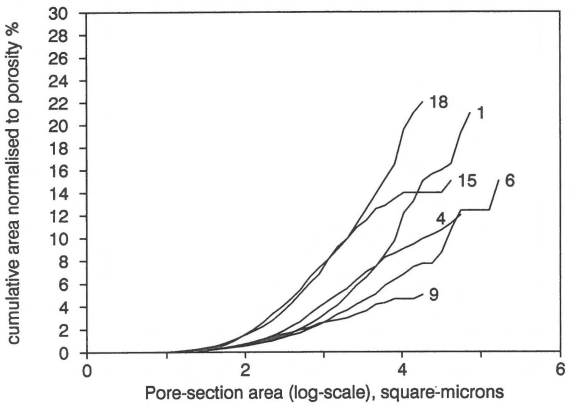

Fig. 14. Examples of cumulative curves (with sample numbers) for the pore area, related to the pore section size classes (log-scale). Two samples (15 and 18) are described to have a large fraction of small pores. This clearly shows up on the cumulative curves, and differentiates these samples. The other samples (1, 4, 6 and 9) include a large fraction of large mouldic pores.

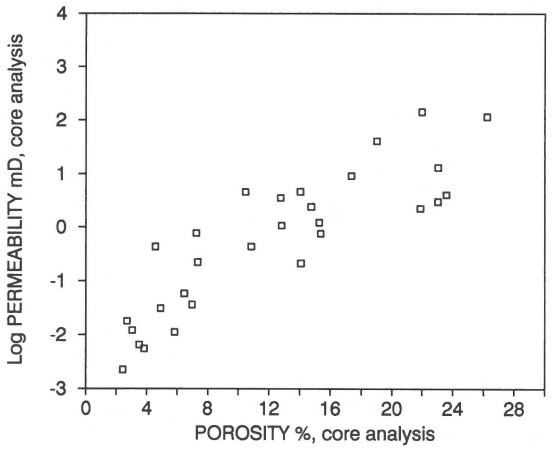

Fig. 15. Relation between core analysis porosity and permeability (log-scale). The scatter indicates differences in pore geometry or heterogeneous samples.

ple, samples such as no. 15 and 18 (Fig. 14) show cumulative curves with an important contribution from the small pore size fraction.

The porosity/permeability relationship in the sample suite (Fig. 15) shows a scatter around a linear trend. Comparison of the Specific Surface measured by image analysis of the permeability (Fig. 16) shows a fairly linear relationship. This indicates that the influence of pore geometry on flow processes is fairly well reflected in the measure of Specific Surface in these samples, even though the permeability ranges from less than 0.01 to 100 mD. This relationship has also been described by Habesch (1990).

Conclusions

Image analysis is a technique that can be used to measure porosity in specific parts of a given sample and thus has a potential to investigate quantitatively small-scale heterogeneities. The ability to quantify parameters of individual pore sections and to derive average values for bulk characteristics makes it a useful tool in relating pore geometry to other petrophysical data.

The Specific Surface and Surface Density measurements of pores can be used to estimate permeability and to characterize mouldic porosity in the Zechstein carbonates studied.

The cumulative porosity curves related to pore section area classes can be used to outline suites of samples with different amounts of small pores.

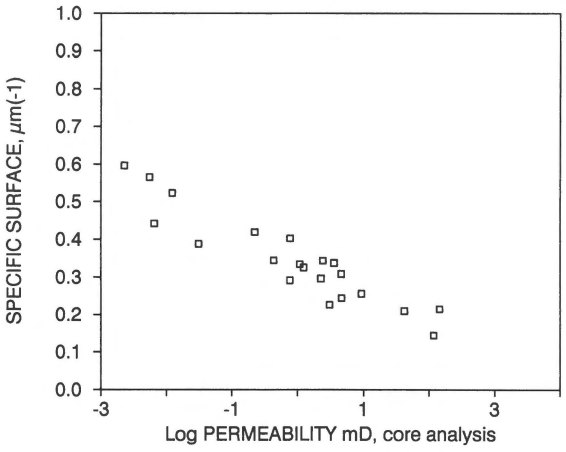

Fig. 16. Relation between core analysis permeability (log-scale) and Specific Surface measured by image analysis. Specific Surface seems to estimate permeability in a broad range from less than 0.01 to 100 mD.

Acknowledgement

Torsten Hoelstad at the Geological Image Analysis Laboratory at Geol. Surv. Denmark is thanked for cooperation and useful discussions. The Scanning Electron Microscope Laboratory at Geological Institute, University of Copenhagen, is gratefully acknowledged for providing SEM-facilities. The main part of this work was carried out under a research project supported by the EEC (contract no. EN3C/0030-DK).

References

Bisdom, E.B.A., H.A. Van Adrichem Boogaert, G. Heintzberger, D. Schoonderbeek & F. Thiel 1983 Porosity measurements and form analysis of mineral grains in thin sections from oil-gas reservoir rocks using Quantimet 720 and BESI – Geoderma 30: 323–337

Delesse, M.A. 1847 Procédé mécanique pour déterminer la composition des roches – C.R. Acad. Sci. 25: 544

Dilks A. & S.C. Graham 1985 Quantitative mineralogical characterization of sandstones by back-scattered electron image analysis – J. Sed. Petrol. 55 (3): 347–355

Dullien, F.A.L. & G.K. Dhawan 1973 Photomicrographic size distribution determination of non-spherical objects – Powder Technol. 7: 305–313

Dullien, F.A.L. & G.K. Dhawan 1974 Characterization of pore structure by a combination of quantitative photomicrography and mercury porosimetry – J. Colloid Interface Sci. 47 (2): 337–349

Ehrlich, R., S.J. Crabtree, S.K. Kennedy & R.L. Cannon 1984 Petrographic image analysis. I. Analysis of reservoir pore complexes – Jour. Sed. Petrol. 54 (4): 1365–1378

Ehrlich, R., S.J. Crabtree, K.O. Horkowitz & J.P. Horkowitz 1991 Petrography and reservoir physics I: Objective classification of reservoir porosity – Amer. Assoc. Petrol. Geol. Bulletin 75 (10): 1547–1562

Frykman, P., N. Stentoft, K.L. Rasmussen, O.W. Christensen, P.V. Andersen & F.L. Jacobsen 1989 Diagenesis and porous system in Danish Zechstein carbonate reservoirs – CEC Report No. EUR 12446 EN. Luxembourg: Office for Official Publications of the European Communities, 167 pp

Gundersen, H.J.G. 1986 Stereology of arbitrary particles – Jour. of Microscopy 143 (1): 3–45

Habesch, S.M. 1990 The evaluation of pore-geometry networks in clastic reservoir lithologies using microcomputer technology. In: J.T. Hanley & D.F. Merrian (eds) Microcomputer Applications in Geology. II. Computers & Geology, Vol. 6: 91–110

Rink, M. & J.R. Schopper 1978 On the application of image analysis to formation evaluation – The Log Analyst. Jan-Feb 1978: 12–22

Ruzyla, K. 1986 Characterization of pore space by quantitative image analysis – Soc. Petrol. Eng. Formation Evaluation, August 1986: 389–398

Stemmerik, L. & P. Frykman 1989 Stratigraphy and sedimentology of the Zechstein carbonates of southern Jylland, Denmark – Danm. Geol. Unders. Series A, Nr. 26, 32 pp

Stentoft, N. 1990 Diagenesis of the Zechstein Ca-2 carbonate from the Løgumkloster-1 well, Denmark – Danm. Geol. Unders., Serie B, No. 12, 42 pp

Stentoft, N. & E. Nygaard 1986 Løgumkloster-1. Diagenesis and sedimentology of the Zechstein Ca-2 carbonates in the Løgumkloster-1 well, Denmark – Report no. 22. Geol. Surv. of Denm. 96 pp

Yuan, L. 1990 Pore image characterization and its relationship to permeability – Society of Core Analysts Annual Technical Conference paper 9002, Dallas, Texas, Aug. 14–16, 18 p